Pullout of steel fibres from a refractory castable: experiment and modelling

Emmanuel Cailleux, Thierry Cutard, Gérard Bernhart

Pullout of steel fibres from a refractory castable: experiment and modelling

E. Cailleux [a,*], T. Cutard [b,*], G. Bernhart [b]

[a] *Laboratoire de Recherche des Monuments Historiques, 29 rue de Paris, 77420 Champs-sur-Marne, France*
[b] *Ecole des Mines d'Albi Campus Jarlard-Route de Teillet, 81013 Albi, France*

Abstract

The pullout behaviour of steel fibres from a refractory castable was characterized through high temperature pullout tests and scanning electron microscopy observations. The effects of the firing temperature, the testing temperature and the inclination angle on the pullout performances were quantified. Complementary optical microscopy observations allowed to identify the pullout micromechanisms induced by the fibre inclination angle such as fibre bending, matrix spalling and the development of a concentrated friction load at the fibre exit point from the matrix. From these results, an analytical pullout model of inclined fibre was developed. The model is based on the strength of materials theory and takes into account the pullout micromechanims previously described. Two domains are considered. The first one corresponds to the free fibre length outside the matrix and models the fibre bending. The second one corresponds to the embedded fibre segment and manages the concentrated friction load, the fibre extraction and the matrix spalling. A good agreement was obtained between the predicted and the experimental pullout curves for all the considered conditions of firing and testing temperatures. A parametric study was then performed. The effects of the friction coefficient, the fibre Young's modulus, the concrete rupture strength and the testing temperature on the pullout performances were quantified and discussed.

Keywords: Refractory castable; Pullout; Modelling; Steel fibre; Inclination angle; High temperature testing

1. Introduction

As cementitious materials, the macromechanical behaviour of refractory concrete is quasi-brittle. Nevertheless, incorporation of metallic fibres can significantly improve their mechanical performances in terms of toughness, pseudo-ductility,

* Corresponding authors. Tel.: +33 1 60 37 77 86; fax: +33 1 60 37 77 99 (E. Cailleux), tel.: +33 5 63 49 31 61; fax: +33 5 63 49 30 99 (T. Cutard).

E-mail addresses: emmanuel.cailleux@culture.gouv.fr (E. Cailleux), cutard@enstimac.fr (T. Cutard).

and energy absorption capacity. In such composites, fibres act as bridging ligaments behind the crack tip and limit the crack propagation. Moreover, in practice, the fibres in fibre reinforced concretes are shortfibres with a quasi-random distribution in the matrix. Fibres at any angle can therefore intersect cracks (Bartos, 1982; Shah and Ouyang, 1991).

Several authors have experimentally shown that the inclination angle of a fibre in a cementitious material has a strong influence on the pullout resistance and consequently on the composite mechanical properties at a macromechanical scale. This orientation effect was observed for metallic (Morton and Groves, 1974; Naaman and Shah, 1976; Ouyang et al., 1994), polymeric (Katz and Li, 1995; Li et al., 1990) and ceramic fibres (Bartos, 1982; Helfet and Harris, 1972). Except for brittle fibres, an increase of both pullout load and pullout energy was generally observed when increasing the inclination angle. Furthermore, most authors concluded that an optimal inclination angle can be determined for which the load and the energy absorption capacity are maximal. Otherwise, an evolution of this optimal orientation angle was observed in agreement with material properties and fibre shape (Morton and Groves, 1974; Li et al., 1990; Helfet and Harris, 1972; Bartos and Duris, 1994).

Advanced investigations of the fibre/matrix behaviour during pullout tests provided phenomenological descriptions of mechanisms inducing pullout load variation with inclination angle. Using a transparent resin matrix with birefringence properties, Morton and Groves (1974) observed the bending of the fibre and a compression yielding of the matrix near the exit point of the fibre. Moreover, Li et al. (1990) noticed a spalling of the concrete matrix near fibre exit and an increase of the pullout load with the inclination angle; analysis of these experimental tests showed that pullout load variations can be attributed to a local concentration of friction load. These experimental investigations of the inclination effect demonstrated that, in addition to debonding and friction, new pullout micromechanisms occur such as fibre bending, matrix spalling and concentration of friction load. It appears from literature that contributions of these mechanisms depend on material properties and inclination angle. Besides, major tendencies can be drawn. Increase of matrix spalling (Morton and Groves, 1974; Helfet and Harris, 1972; Khanna and Shukla, 1994) and decrease of pullout fibre length (Li et al., 1990; Cai and Faber, 1992) were also generally noticed when inclination angle increases.

Optimization of the composite macromechanical behaviour by adjusting the properties and geometry of the fibre is the main motivation to develop micromechanical modelling taking into account the pullout mechanisms described above. Nevertheless, few micromechanical pullout modellings of inclined fibres were proposed.

In the model presented by Morton and Groves (1974), the fibre is considered as a cantilever beam and the matrix is assumed to be in compression near the fibre exit point. This model can predict the maximum force needed to produce a given deflection of an elastic or perfectly plastic fibre. Nevertheless, the debonding and the friction load for pullout of a straight fibre are neglected. As a consequence, pullout load is zero which differs obviously from experimental results.

The model of Li et al. (1990) assumes an exponential increase of the pullout load with inclination angle. The authors introduce a "snubbing factor" taking into account the local concentration of friction load provided by fibre inclination. This model shows good agreement with experimental results obtained when extracting inclined polymeric fibres. However, as mentioned by Leung and Chi (1995), only the maximum pullout load can be obtained and no modelling of pullout load evolution with fibre displacement is performed. Moreover matrix spalling and fibre bending are not considered even if experimentally observed.

These mechanisms were introduced by Leung and Li (1992) using a finite-element modelling. Firstly developed for brittle fibres and later extended by Leung and Chi (1995) for ductile fibres, this model requires two computation steps. Considering the fibre embedded in the matrix as a beam on an elastic foundation, the first finite-element calculation aims to get the foundation stiffness and matrix spalling criterion along the fibre embedded length. The bending load needed to produce the fibre displacement is computed in the sec-

ond step. Also, a debonding model can be implemented in this approach and the total pullout load is then obtained by addition of the debonding and of the bending contributions. Even though the model predictions are in good agreement with experimental data, the modelling does not take into account the concentration of friction load and leads to underestimate the pullout load at low angles. It should be noted that the accuracy of the spalling effect depends on the mesh used.

Recently, two analytical approaches were respectively proposed by Katz and Li (1995), and by Leung and Ybanez (1997). Katz and Li (1995) model the debonding and the fibre bending mechanisms in a coupled approach. As the model of Leung and Li (1992), the fibre is considered as a beam supported on an elastic foundation. The model of Leung and Ybanez (1997) is based on the same approach of the model of Li et al. (1990) and defines a "snubbing friction coefficient". Matrix spalling at the fibre exit point is considered in these models too. Even if good agreements are obtained between the predicted and the experimental pullout curves for the two models, these are based on phenomenological developments for which several empirical constants are introduced and estimated from experimental curves. Therefore, numerous pullout tests at different inclination angles are necessary to identify the model constants.

The main objective of the research presented in this paper is to propose an analytical pullout modelling which can predict both the complete pullout load versus displacement curve and the pullout energy for fibres at any inclination angle. The model is applied to a refractory concrete reinforced by metallic fibres for application temperatures close to 500 °C. Pullout micromechanisms such as fibre bending, matrix spalling and local concentration of friction load are taken into account in the model. More attention is paid to base the model of these pullout micromechanisms on physical approaches deduced from experimental pullout tests and microscopic observations of the fibre/matrix interfaces. Effects of firing temperature and testing temperature on the pullout behaviour are respectively characterized by the way of room temperature pullout tests and high temperature pullout tests. A parametric study is then performed to quantify and to discuss the effect of material properties, firing temperature and testing temperature on the fibre reinforcement efficiency.

2. Experiments

2.1. Materials and testing set-up

The refractory concrete matrix consisted of an inorganic alumino-silicate binder phase and of cordierite aggregates. The binder phase was obtained by mixing a solid and a liquid precursors (Davidovits, 1999). The solid one consisted of a major alumino-silicate oxide and of thermal silica fume. The liquid precursor was an aqueous solution of potassium polysilicate. Aggregates consisted of a mixture of four granulometric ranges (0–125 μm, 0.2–0.5; 0.5–1.5; 1.5–3 mm) of a commercial cordierite grog. The refractory concrete was shaped first by mixing these different components and then by casting under vibrations. Complete polymerisation of the binder phase was obtained after an isothermal heat treatment of 12 h at 80 °C. The resulting reaction product had a chemical composition close to that of the orthoclase mineral phase $K(AlSi_3)O_8$. During the first heating, large microstructural transformations occurred in the refractory concrete matrix (Cutard et al., 1999; Cailleux, 2001). Like their consequences on the mechanical properties, they were presented in a previous paper (Cutard et al., 1999; Cailleux et al., 2002a,b). For applications as moulds in the SPF process and in order to stabilise the microstructure, this refractory concrete had to be previously fired at 500 °C for shaping Al parts and at 980 °C for shaping Ti parts.

Metallic fibres were made of an AISI 310 stainless steel and were processed by cold drawing. Three diameters were considered in the present work: 0.38, 1 and 2 mm. The embedded fibre extremity was mechanically polished in order to ensure the reproducibility of the fibre/matrix interface quality at this specific location. Pullout sample were elaborated by following the processing route of the refractory castable and after fitting the fibre in the casting mould. Cylindrical sample dimen-

sions were 25 mm in diameter and 80 mm in length. Two fibre embedded lengths were considered: 6 and 12 mm. With respect to the polymerisation process of the binder phase and to the application temperature of the superplastic forming process (SPF), the 80, 500 and 980 °C firing temperatures were retained for these pullout samples. The mechanical properties both of the refractory concrete and of the metallic fibres were previously characterized through room temperature and high temperature mechanical tests (Cailleux et al., 2002a,b; Cutard et al., 1999; Cailleux, 2001).

Pullout tests were performed on an INSTRON 4467 device equipped with a 500 N load cell. Fig. 1 shows the pullout test in the high temperature configuration. Sample base was glued to the upper water-cooled plate and the fibre extremity was fitted in a lower tensile grip. The fibre extraction was measured with a high temperature extensometer. Pullout tests were carried out at a constant extraction velocity of 0.5 mm/min and with a periodic acquisition of both the extraction load and fibre displacement. Heating was made by a MTS 653 furnace with two heating zones. Thermal gradient was measured in the 12 mm area of the fibre embedded length and was less than 1 °C at 500 °C.

2.2. Pullout curves and fibre inclination angle effect

Fig. 2 shows load–displacement curves obtained during the extraction of straight fibres of 2 mm in diameter. Four test configurations are considered: three ones (A, B and C) correspond to room temperature tests performed after firings at 80, 500 and 980 °C and the fourth one (D) consists of a 500 °C temperature test performed after a firing at 500 °C. Two conventional domains can be distinguished on these experimental pullout curves: the debonding domain (1) which presents a regular increase of the extraction load up to the maximum load F_{pic} and the friction domain (2).

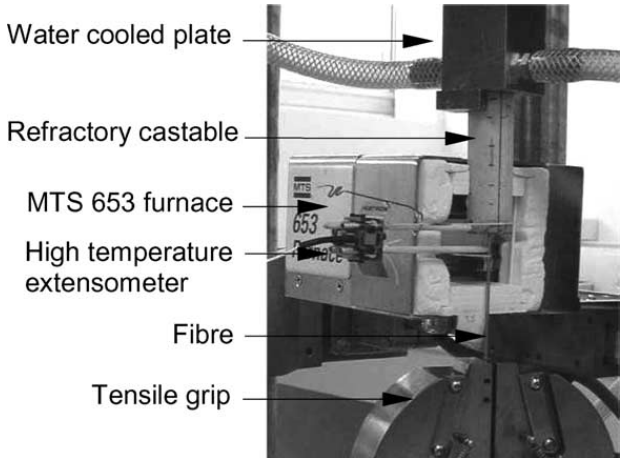

Fig. 1. High temperature pullout test (opened furnace).

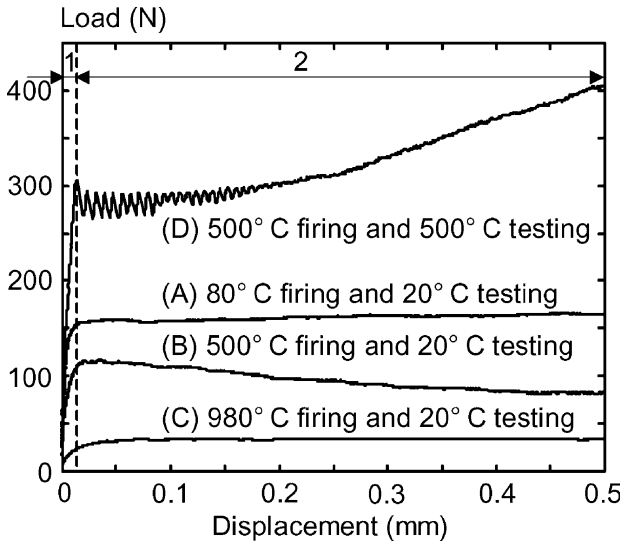

Fig. 2. Influence of the testing and the firing temperatures on the pullout behaviour for a 2 mm fibre diameter.

The firing temperature and the testing temperature affect principally the pullout load level. Concerning the firing temperature, Fig. 2 shows that an increase of this parameter leads to an important decrease of F_{pic} and of the friction load. Complementary observations performed by scanning electron microscopy (SEM) showed that the heat treatment induces a damage of the refractory matrix combined with a decohesion of the fibre/matrix interface. Fig. 3 illustrates the evolutions of the composite microstructure after a 500 °C heat treatment: numerous cracks can be noticed in the cement paste and at the cement/aggregate interfaces. Radial cracks and fibre/matrix decohesions can also be observed all around the fibre. As developed in Cailleux et al. (2002a,b), it was demonstrated that a significant stress field is generated near the fibre/matrix interface during the first heat-

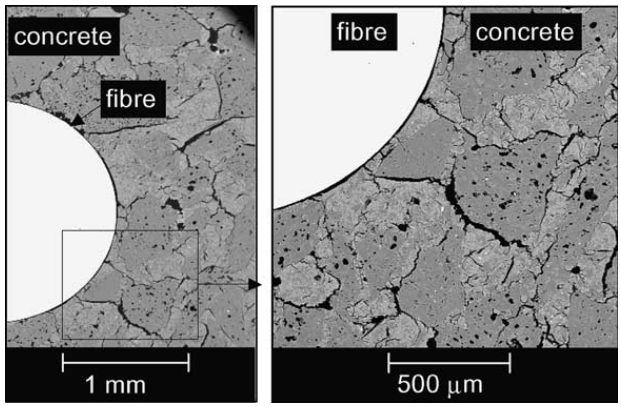

Fig. 3. SEM micrographs of a fibre/matrix interface after a 500 °C firing.

ing due to the thermal expansion mismatch between the matrix and the steel fibre. Analytical estimation of this stress field indicated that the tangential stress component exceeds the tensile matrix rupture stress. As a consequence, it can be concluded that the firing step induces both a matrix cracking and a fibre/matrix decohesion. These damage mechanisms increase with the firing temperature and are responsible of the decrease of the pullout strength.

Concerning the testing temperature, a significant increase of the maximum debonding load F_{pic} and of the friction load in domain 2 is observed in Fig. 2 when this parameter increases. For a test temperature of 500 °C, the pullout load level is more than six times the load level obtained at room temperature after the same 500 °C firing treatment. This phenomenon is the result of the development of a fretting pressure generated by the thermal expansion mismatch between the concrete and the steel fibre. As a consequence, a supplementary load has to be applied to extract the fibre. As described in Cailleux et al. (2002a,b), this mechanism can be explained by considering the pullout load required in a high temperature test as the sum of two components: the first one allowing to extract the fibre without any fretting pressure and the second one corresponding to a supplementary load taking into account the fretting pressure induced by the testing temperature and the radial fibre contraction due to the Poisson effect. The emergence of a stick-slip mode at the beginning of the friction domain is noticed in Fig. 2 too. Previous work demonstrated that such stick-slip mechanisms can be induced by the normal pressure around the fibre, the system stiffness or the extraction velocity (Baumberger et al., 1994, 1995). As the two last parameters were kept constant in all the tests configurations, it can be deducted that the fretting pressure developed at high temperature is responsible of this evolution.

Fig. 4 shows the experimental pullout curves obtained for fibre of 0.38 mm in diameter with inclination angles of 15°, 30°, 45° and 60°. These tests were performed at room temperature after a firing at 80 °C. The fibre inclination induces several strong evolutions of the pullout curve but a debonding and a friction domain can still be defined.

The first noticed evolution concerns the pullout load. In the debonding domain (1), an increase of F_{pic} is observed with the fibre inclination up to an angle of 45°. Beyond this value, the maximum debonding load decreases. A similar evolution is obtained in the friction domain (2): the friction load increases with the fibre inclination up to 45° and decreases for higher angle values. As a consequence, it can be concluded that an optimal inclination angle for which the extraction load is maximal could be determined in the 30–60° inclination domain.

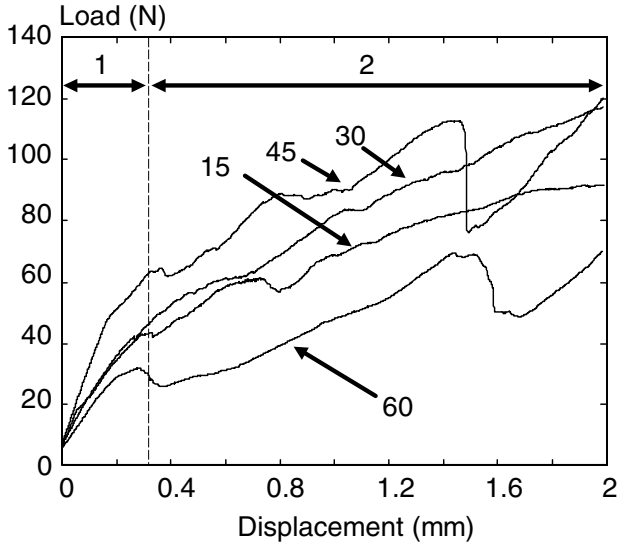

Fig. 4. Pullout curves obtained at room temperature with fibre inclinations of 15°, 30°, 45° and 60°.

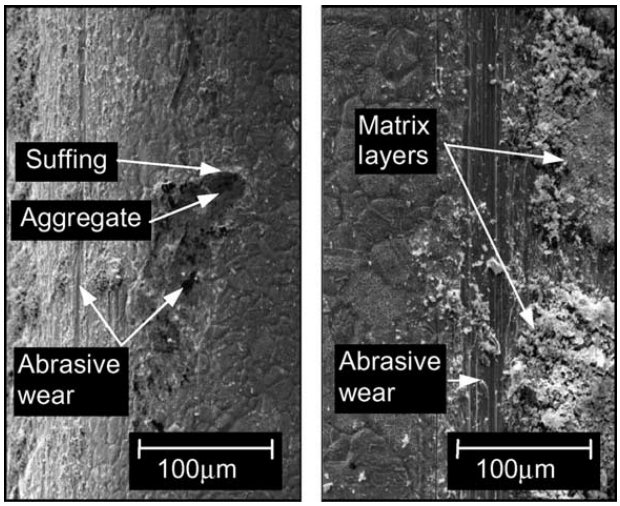

Fig. 5. SEM micrographs of the fibre surface after 20 °C pullout tests on samples fired at 980 °C.

The second evolution concerns the shape of the pullout curve: a trend of increase of the friction load is observed throughout the friction domain. This particular evolution can be explained with the help of SEM observations of the fibre surface after a room temperature pullout test (Fig. 5). In these micrographs, numerous thin layers of matrix adhering to the fibre surface and several matrix particules embedded in the fibre structure can be noticed. Local fibre plastic deformations and abrasive wear mechanisms induced by hard matrix particules are clearly identified too. Such mechanisms can clearly contribute to increase the pullout load during the fibre extraction process.

Several load drops can be observed in the pullout curve of inclined fibre too. The number and the amplitude of these load drops increase with the inclination angle. Completing the recording of the load and displacement components by visual observations of the sample during the pullout test, it was established that these load drops are due to the spalling of small concrete blocks localized at the fibre exit point from the matrix.

2.3. Pullout energy

Fig. 6a shows the evolution of the pullout energy as a function of the inclination angle for the 80, 500 and 980 °C firing temperature. The energy was calculated as the area under the load–displacement pullout curve. For the three considered firing conditions, the evolution of the pullout energy as a function of the inclination angle is similar to the evolution of the pullout load: the pullout energy increases up to a maximal energy point reached for an inclination angle within the 30–45° range and decreases for higher inclination values. This evolution confirms the effect of the fibre inclination on the pullout mechanical performances noticed on the load–displacement curves. In addition, it is possible to conclude that an optimal angle for which the extraction energy is maximum can be

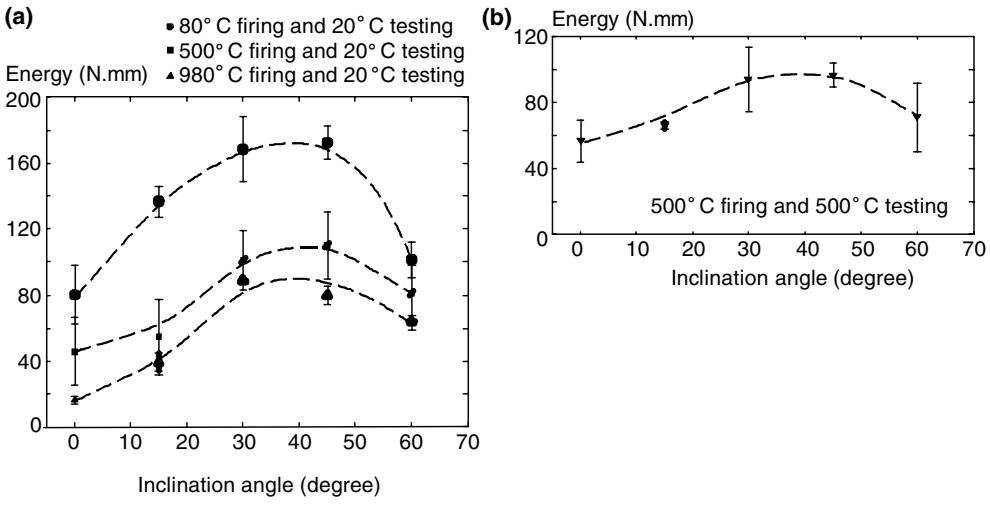

Fig. 6. Evolution of the pullout energy as a function of the inclination angle. (a) Room temperature tests—fibre embedded length of 12 mm and (b) high temperature tests—fibre embedded length of 6 mm.

determined. This optimal inclination angle is close to 40° for the three considered firing temperatures.

The decrease of the pullout performances when increasing the firing temperature is confirmed by the determination of the pullout energies (Fig. 6a). The maximal pullout energies are obtained after 80° firings and the minimal ones corresponds to the 980 °C firings.

The combined effect of the fibre inclination and the testing temperature was quantified too (Fig. 6b). The embedded fibre length used in these tests was 6 mm. In the case of a 12 mm embedded fibre length, the rupture of the fibre was systematically obtained for inclination angles higher than 15°. For these high temperature tests, even if the embedded fibre length is two times lower, a significant increase of the pullout energy can be observed in comparison to the room temperature tests performed after a 500 °C firing. As described above, such a benefit effect must be attributed to the development of a fretting pressure at the fibre/matrix interface due to the thermal expansion mismatch between the matrix and the steel fibre.

2.4. Pullout micromechanisms

Several pullout micromechanisms induced by the fibre inclination angle were identified by the observation of polished sections of tested pullout samples. Fig. 7 shows an example of such a pullout sample section for a fibre inclined at 45° with respect to the pullout axis. The matrix spalling and the fibre bending mechanisms can be clearly identified. It can be noticed that the matrix spalling mechanism occurs perpendicularly to the embedded fibre axis. Moreover, it is observed that after spalling of a matrix element, the fibre exit point (E) is moved from the pullout axis and that the free fibre length is increased of the spalling element length.

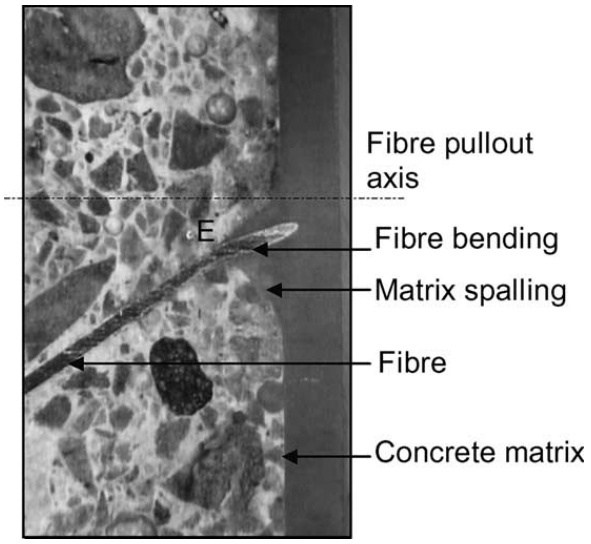

Fig. 7. Identification of the pullout micromechanisms from a polished section of a tested pullout sample.

3. Pullout modelling

3.1. General methodology

The developed micromechanical model is an analytical model based on the strength of materials theory. The modelled mechanical system is close to the experimental pullout configuration. In the experimental test, one part of the fibre is inclined and embedded in the matrix and the other part is constituted of a free fibre length whose extremity is fitted into a tensile grip. In this way, the modelled system is assumed to be composed of the two domains described in Fig. 8.

The first domain (domain 1) only considers the free fibre length between the fibre exit point (E) and the tensile grip (B). This part is composed of the initial free fibre length (A–B) and of to the fibre length extracted during the test (A–E). These two fibre segments are modelled as two beams connected by a common junction (node A). The fibre exit point (E) from the matrix is considered as a fixed end. The mechanical system can deform by bending when a displacement of the fibre extremity (B) is imposed. Reaction loads generated in the fixed end (E) are calculated and used in the second domain (domain 2) of the model.

The second domain (domain 2) corresponds to the inclined fibre length embedded in the matrix. From the reaction loads calculated in domain 1 at the fibre exit point (E), the consideration of domain 2 allows to predict the matrix spalling, the fibre extraction and the amplitude of the local friction load. Concerning fibre extraction and matrix

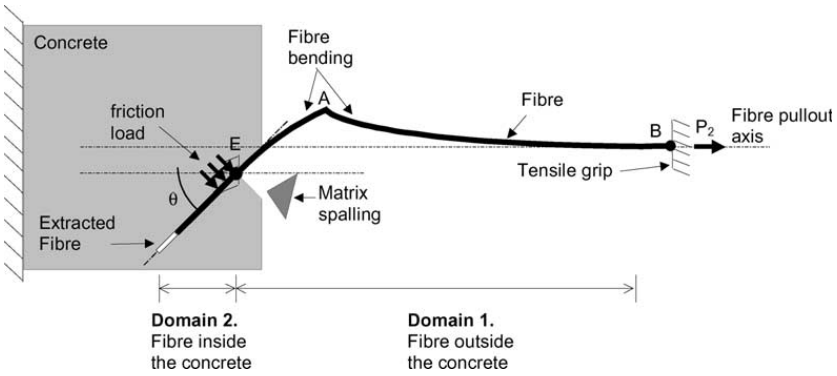

Fig. 8. Schematical description of the developed micromechanical model.

spalling mechanisms, critical strength values are fixed in the model. Comparison of calculated loads with these critical strength allows to predict fibre extraction or matrix spalling.

3.2. Detailed description of the pullout model

3.2.1. Domain 1—Free fibre segment

Modelling of the two beams system constituting this part was developed in two steps with the aim of managing the pullout process by an imposed displacement of fibre extremity (B). In *step one*, reaction loads at the fixed end (E) are calculated as a function of loads applied at the fibre extremity (B). Displacement of that extremity induced by the bending of the two beams system is then deduced. In *step two*, analytical relationships are expressed as a function of the fibre extremity (B) displacement.

3.2.1.1. Step one—Analytical expressions of the reaction loads generated in the fixed end (E). Pullout load is assumed to be a combination of two load components applied at fibre extremity (B). As shown in Fig. 9, the first one (P_1) is applied perpendicularly to the fibre pullout axis and is necessary to maintain the fibre end (B) on the pullout axis. The second one (P_2) is applied along the pullout axis. It corresponds to the fibre extraction load imposed by the displacement of the tensile grip during the pullout test (Fig. 10).

As illustrated in Fig. 9, a bending of the two beams system associated with a displacement (d_{P1}) of the fibre extremity occurs when P_1 is applied. The considered configuration is the more general one, i.e., fibre extraction and matrix spalling are taken into account. In these conditions, the initial fibre geometry described in Fig. 9 shows that the fibre end (B) and the fibre exit point from

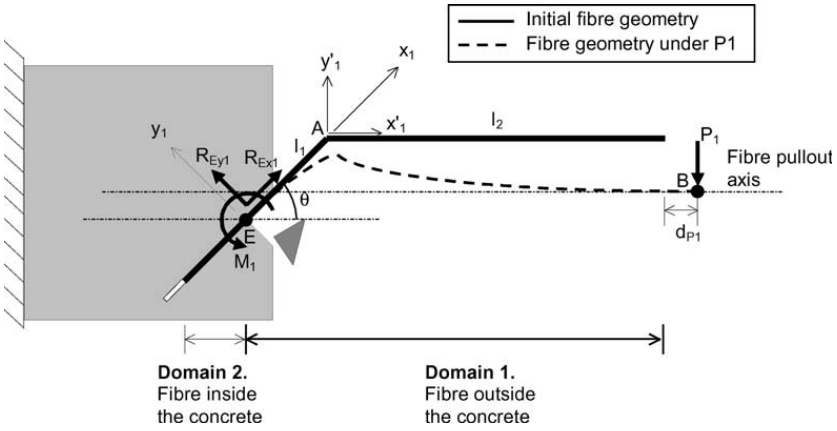

Fig. 9. Modelling of domain 1 (step 1): deformation of the two beams system and reaction loads generated in the fixed end (E) by the application of P_1.

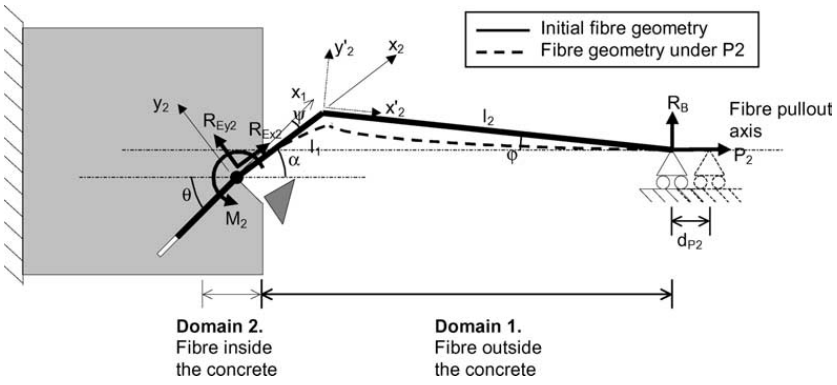

Fig. 10. Modelling of domain 1 (step 2): deformation of the new beams system and reaction loads generated by the application of P_2.

the matrix (E) are not aligned with the pullout axis. In Fig. 9, the fibre segment (A–B) of length l_2 corresponds to the free initial fibre length outside the matrix. The fibre segment (E–A) of length l_1 appears after fibre extraction and/or matrix spalling. Inclination angle of the embedded fibre length is θ with respect to the pullout axis.

Reaction loads R_{Ex1}, R_{Ey1} and M_1 are generated by P_1 at the fixed end (E). Analytical expressions of these reaction loads are obtained by the strength of materials theory and correspond respectively to Eqs. (1)–(3). These expressions are calculated in the coordinates system $(x_1,\ y_1)$. Deflection of the beam (E–A) is calculated in the coordinates system $(x_1,\ y_1)$ and deflection of the beam (A–B) is calculated in the coordinates system (x_1', y_1'). Deflections of the beams (E–A) and (A–B) are given respectively by Eqs. (4) and (5) with $x_1 = l_1$ and $x_1' = l_2$. Displacement d_{P1} of the fibre extremity is obtained by Eq. (8).

$$R_{Ex1} = P_1 \sin(\theta) \tag{1}$$

$$R_{Ey1} = P_1 \cos(\theta) \tag{2}$$

$$M_1 = P_1(l_1 \cos(\theta) + l_2) \tag{3}$$

$$y_{P1l1} = \frac{P_1}{E_f I_z}\left(\frac{l_2 l_1^2}{2} - \frac{l_1^3 \cos(\theta)}{3}\right) \tag{4}$$

$$y_{P1l2} = \frac{P_1 l_2^3}{3E_f I_z} + \frac{C_1 l_2}{E_f I_z} + \frac{C_2}{E_f I_z} \tag{5}$$

$$C_1 = -P_1\left(\frac{l_1^2 \cos(\theta)}{2} + l_2 l_1\right) \tag{6}$$

$$C_2 = P_1 \cos(\theta)\left(\frac{l_2 l_1^2}{2} - \frac{l_1^3 \cos(\theta)}{3}\right) \tag{7}$$

$$d_{P1} = -y_{P1l1} \sin(\theta) \tag{8}$$

Following the application of P_1, the two beams system is assumed to be deformed in a bending mode. Nevertheless, this final configuration must be simplified to model the action of the pullout load P_2. For this reason the new mechanical system described in Fig. 10 is considered. This one is constituted of the two straight beams (E–A) and (A–B), respectively inclined of angles α and φ with respect of the fibre axis. A new axes system $(x_2,\ y_2)$ turned of an angle ψ with respect of the initial axes system $(x_1,\ y_1)$ is defined too. Moreover, the modelling still considers the case of fibre extraction and matrix spalling. In this way, the fibre exit point is not aligned with the pullout direction (Fig. 10).

Fig. 10 illustrates the deformation of the new beams system induced by the application of P_2. In addition to the fixed end considered at the fibre exit point (E), a support is added to the mechanical system to fix the fibre extremity (B) on the pullout axis. Reaction loads R_{Ex2}, R_{Ey2} and M_2, generated in the fixed end (E), are given by Eqs. (9)–(11). They were calculated in the axes system $(x_2,\ y_2)$. Deflections of the beams l_1 and l_2 correspond respectively to Eqs. (12) and (13). Deflection of the beam (E–A) is calculated in the axes system $(x_2,\ y_2)$ and deflection of the beam l_2 was calculated in the axes system (x_2', y_2'). Furthermore, as the two beams (E–A) and (A–B) are connected, deflection of beam (A–B) can be expressed as a

function of the deflection of the beam (E–A). Displacement d_{P2} of the fibre extremity is obtained by Eq. (14). It is composed of displacement d_{Pl1} induced by deflection of (E–A) and of displacement d_{Pl2} caused by deflection of (A–B). In these equations, analytical expression of R_B is determined assuming a zero fibre deflection at the extremity of segment (A–B).

$$R_{Ex2} = -P_2\cos(\alpha) - R_B\sin(\alpha) \tag{9}$$

$$R_{Ey2} = P_2\sin(\alpha) - R_B\cos(\alpha) \tag{10}$$

$$M_2 = P_2(l_1\sin(\alpha) - l_2\sin(\varphi)) - R_B(l_1\cos(\alpha) + l_2\cos(\varphi)) \tag{11}$$

$$y_{P2l1} = \frac{-P_2 l_1^2}{2E_f I_z}(l_1\sin(\alpha) - l_2\sin(\varphi)) + \frac{R_B l_1^2}{2E_f I_z}(l_1\cos(\alpha) + l_2\cos(\varphi)) + \frac{l_1^3}{6E_f I_z}(P_2\sin(\alpha) - R_B\cos(\alpha)) \tag{12}$$

$$y_{P2l2} = y_{P2l1}\frac{\cos(\alpha)}{\cos(\varphi)} \tag{13}$$

$$\begin{aligned} d_{P2} &= d_{P2l1} + d_{P2l2} \\ &= y_{P2l1}\sin(\alpha) + y_{P2l2}\sin(\varphi) \\ &= y_{P2l1}\sin(\alpha) + y_{P2l1}\cos(\varphi)\tan(\varphi) \end{aligned} \tag{14}$$

The complete reactions loads R_{Extot}, R_{Eytot}, M_{tot} generated in the fixed end (E) are respectively given by Eqs. (15)–(17). They are expressed in the axes system (x_1, y_1) and were obtained by summing the reaction loads generated by P_1 and P_2. As the loads R_{Ex2}, R_{Ey2} are expressed in the axes system (x_2, y_2), their components in the axes system (x_1, y_1) were first calculated and then added to the reaction loads R_{Ex1} and R_{Ey1}.

$$R_{Extot} = R_{Ex1} + R_{Ex2}\cos(\psi) + R_{Ey2}\sin(\psi) \tag{15}$$

$$R_{Eytot} = R_{Ey1} - R_{Ex2}\sin(\psi) + R_{Ey2}\cos(\psi) \tag{16}$$

$$M_{tot} = M_1 + M_2 \tag{17}$$

3.2.1.2. Step two—Expression of pullout load P_2 as a function of the imposed displacement. During experimental tests, fibre extraction is performed by the way of an imposed displacement of the fibre extremity (B). In this step, previous equations are combined in the aim to express the pullout load P_2 as a function of the fibre end displacement (d_{imp}). In a first step, the imposed displacement (d_{imp}) is assumed to be equal to the sum of the displacement provided by P_2 (d_{P2}) plus the fibre elastic deformation (d_{elas}) and plus the displacement provided by P_1 (d_{P1}):

$$d_{imp} = d_{P2} + d_{elas} + d_{P1} \tag{18}$$

Eq. (19) gives the analytical expression of fibre displacement induced by elastic deformation where S is the fibre section.

$$d_{elas} = \left(|(-P_2\cos(\alpha) - R_B\sin(\alpha))|\frac{l_1}{E_f S} + |(-P_2\cos(\varphi) - R_B\sin(\varphi))|\frac{l_2}{E_f S}\right) \tag{19}$$

In a second step, substituting Eqs. (8), (14) and (19) into Eq. (18) and rearranging the equation obtained as a function of P_2, expression of the pullout load as a function of fibre extremity displacement (d_{imp}) is determined. This expression is given in Eq. (20).

$$P_2 = \frac{d_{imp} - d_{P1} - d_{elas}}{(l_1^2 C_3 + l_1^2 C_4 + l_1^3 C_5)(\sin(\alpha) + \cos(\alpha)\tan(\varphi))} \tag{20}$$

Constants C_3, C_4 and C_5 are respectively given in Eqs. (21)–(23).

$$C_3 = \frac{(l_1\sin(\alpha) - l_2\cos(\varphi))}{2E_f I_z} \tag{21}$$

$$C_4 = \frac{R_B}{2P_2 E_f I_z}(l_1\cos(\alpha) + l_2\cos(\varphi)) \tag{22}$$

$$C_5 = \frac{\left(\sin(\alpha) - \frac{R_B}{F}\cos(\alpha)\right)}{6E_f I_z} \tag{23}$$

3.2.2. Domain 2—Embedded fibre segment

In this part, reaction loads calculated in domain 1 at the fixed end (E) are used as limit conditions to model concentrated friction load, fibre extraction and matrix spalling.

3.2.2.1. Concentrated friction load modelling. The additional pullout load (F_{sup}) induced by fibre friction is calculated using a Coulomb's model given in Eq. (24). μ, and F_{norm} correspond respectively to the friction coefficient and to the normal load. This normal load is assumed to be composed of the reaction load R_{Eytot} and of a contribution of the moment M_{tot}. It can be assumed that the fibre is fixed on two supports C and D (Fig. 11). In this way, the reaction moment can be decomposed in two equivalent reaction loads R_C and R_D as illustrated in Fig. 11. Eqs. (25) and (26) gives the analytical expressions of these loads where L_0 is the embedded fibre length.

$$F_{sup} = \mu F_{norm} \tag{24}$$

$$R_C = \frac{M_{tot}}{L_0} \tag{25}$$

$$R_D = \frac{-M_{tot}}{L_0} \tag{26}$$

These loads are added to R_{Eytot} to obtain the complete normal load F_{norm} given in Eq. (27).

$$F_{norm} = R_{Eytot} + R_C + |R_D| \tag{27}$$

3.2.2.2. Matrix spalling modelling. The spalling load (F_{spall}) developed at the fibre exit point (E) during fibre extraction is assumed to be composed of the sum of R_{Eytot} plus R_C. The critical load value (F_{rup}) inducing matrix spalling is calculated by assuming that spalling occurs in a bending mode with a fracture section normal to the fibre axis (x_1). The spalling matrix element is supposed to be prismatic as illustrated in Fig. 11. This element is characterized by a length a_1, a height a_2 and a width b_f. The element width (b_f) is supposed to be related to the other dimensions. In this way, for a first spalling, b_f is considered to be equal to $2a_2$ in agreement with experimental observations. For all the next matrix failures, the spalling matrix element length (a_1) is kept constant. Other dimensions are supposed to increase proportionally to the failure number (n). From these assumptions, a general analytical expression of the critical spalling load (F_{rupt}) is determined and given in Eq. (28) where σ_{rupt} is the concrete rupture stress in three points bending. The matrix spalling occurs when F_{spall} is equal or higher to the critical load value F_{rupt}.

$$F_{rupt} = \frac{\sigma_{rupt} n^3 a_1^2}{3\sin(\theta)\tan^2(\theta)} \tag{28}$$

3.2.2.3. Fibre extraction modelling. The fibre is assumed to be extracted if the value of the reaction load R_{Eytot} is higher than a threshold value calculated by the sum of a critical pullout load (F_{crit})

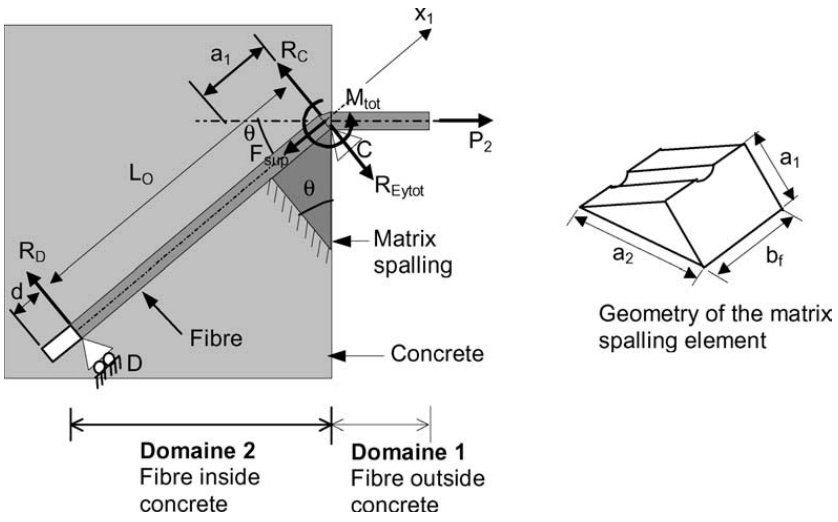

Fig. 11. Modelling of the domain 2: decomposition of the moment M_{tot} in two equivalent loads R_C and R_D and matrix spalling.

plus the load F_{sup} caused by friction. F_{crit} is obtained from the modelling of an experimental curve recorded from the pullout of a straight fibre. This modelling is performed by assuming linear evolutions of the pullout load on the debonding and the friction domains. The debonding domain is thus modelled assuming a linear increase of the pullout load (F_{crit}) as a function of the fibre extremity (B) displacement (Fig. 12). The debonding is complete when the point (F_{pic}, d_{pic}) is reached. A friction pullout mechanism is assumed beyond F_{pic}. The pullout load (F_{crit}) is modelled on this domain as a function of the fibre extremity displacement (d) as following:

$$F_{crit} = ad \quad \text{for } d_{pic} < d \leqslant d_{flim} \tag{29}$$

$$F_{crit} = bd \quad \text{for } d > d_{flim} \tag{30}$$

where a, b and d_{flim} are constants determined empirically.

From the loads F_{pic} and F_{flim}, the shear stresses τ_{pic} and τ_{flim} can be respectively calculated by Eqs. (31) and (32) where r_f is the fibre radius. These shear stresses can be used to model the straight fibre pullout curve in computing configurations for which the embedded fibre length is modified.

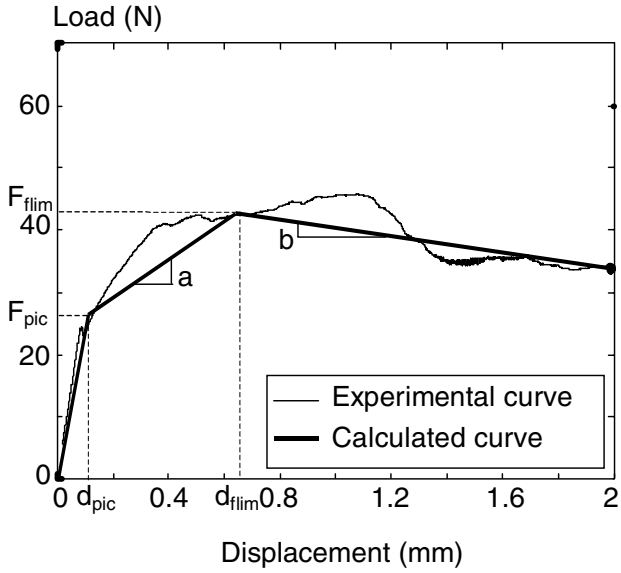

Fig. 12. Modelling of the pullout curve of a non inclined fibre.

$$\tau_{pic} = \frac{F_{pic}}{2\pi r f L_0} \tag{31}$$

$$\tau_{flim} = \frac{F_{flim}}{2\pi r f L_0} \tag{32}$$

3.3. Numerical model implementation

As the analytical equations are expressed as a function of the fibre extremity displacement (B), the numerical model implementation is based on the increment of a constant displacement imposed at that specific point (B). At every increment, numerical tests are performed defining if fibre extraction and/or matrix spalling mechanisms can occur. In this way, the numerical program is composed of several computing loops managing the four next configurations: (1) no fibre pullout and no matrix spalling, (2) matrix spalling and no fibre pullout, (3) fibre pullout and no matrix spalling, (4) fibre pullout and matrix spalling. Numerical treatments of these four cases are described below:

- In case 1, pullout load (P_2) is calculated as a function of the imposed displacement (see Eq. (20)).
- In case 2, the spalled matrix element length is added to the free fibre segment (l_1) and subtracted from the embedded fibre length (l_0).
- In case 3, fibre extracted length is calculated as a function of the imposed displacement value and of the inclination angle θ. This length is added to the free fibre segment (l_1) and subtracted from the embedded fibre length (l_0).
- In case 4, fibre extraction is treated at first as in case 3. Matrix spalling is considered in a second step. The length of the spalled matrix element is added to the free fibre segment (l_1) and subtracted from the embedded fibre length (l_0).

3.4. Model parameter identification

The model is based on the following parameters: fibre radius (r_f), free fibre length (l_2), initial embedded fibre length (l_1), fibre Young's modulus (E_f), friction coefficient (μ), length of the spalled matrix element (a_1), concrete rupture stress in

Table 1
Model parameter values for the different considered configurations

Firing temperature (°C)	Test temperature (°C)	E_f (GPa) at test temperature	Friction coefficient (μ)	τ_{pic} (MPa) at test temperature	τ_{flim} (MPa) at test temperature	L_0 (mm)	a_1 (mm)
80	20	180	0.3	2.47	3.62	12	0.55
800	20	206	0.2	2.08	2.08	12	0.43
500	500	157	0.1	7.3	6	6	0.59

three points bending (σ_{rupt}), and the shear stresses τ_{pic} and τ_{flim}. Table 1 gives the parameter values used for numerical computings corresponding to different firing and test temperatures. A 0.38 mm fibre diameter and a 50 mm free fibre length are considered for three following configurations.

Fibre and matrix properties were determined by tensile and bending tests. In addition, shear stresses were calculated from the curve of a non inclined fibre pullout test. Otherwise, the friction coefficient and the length of the spalled matrix element were determined by comparing the calculated and the experimental pullout curves obtained for a 45° inclination angle. Curves obtained for a fibre inclination of 45° were considered because they present all the pullout mechanisms taken into account in the model.

For these two parameters (μ and a_1), the value which minimizes the difference between the calculated and the experimental curves have been retained. The friction coefficient (μ) is identified as being equal to 0.3 in the case of a drying at 80 °C (Fig. 12). This value is kept constant for all inclinations. A similar procedure was performed to identify friction coefficient values of the different configurations (Table 1).

The length of the spalled matrix element (a_1) was identified as equal to 0.55 considering a 80 °C drying sample. Experimentally, it was observed that an inclination angle increase leads to a regular increase of the total spalled matrix length. In the model, a linear increase of the spalled matrix length is assumed as a function of the inclination angle. As for a straight fibre pullout no matrix spalling occurs, the determination of the length a_1 for a 45° inclination angle allows to calculate the parameter values for any inclination.

4. Model discussion

In a first time, comparisons between predicted and experimental results were performed. In order to validate this modelling, they were made both for room temperature and high temperature pullout tests.

In a second time, parametric studies of the effect of Young modulus variations, concrete rupture stress variations and of the test temperature on the pullout energy were performed too.

4.1. Comparison of model predictions with experimental results

Figs. 13 and 14 compare experimental and predicted pullout curves for fibres inclined at 60°. Experimental tests were performed respectively at

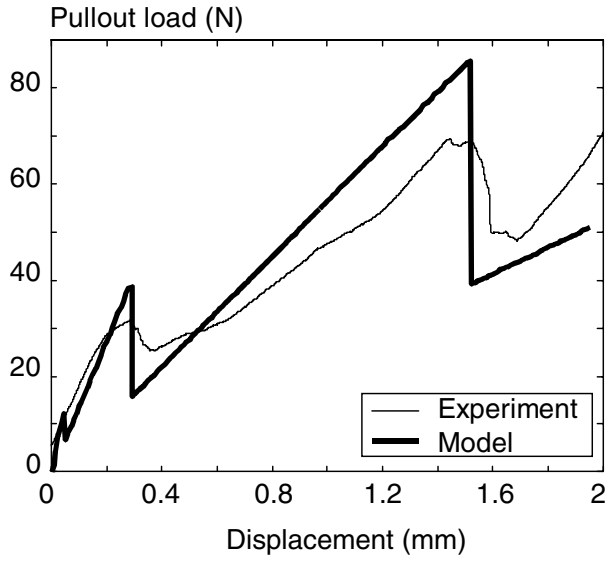

Fig. 13. Comparison of predicted and experimental pullout curves obtained at 20 °C after a 80 °C firing for a fibre inclination angle of 60°.

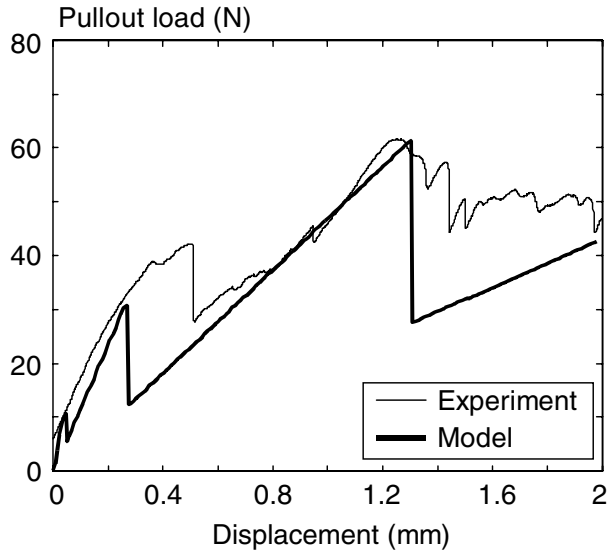

Fig. 14. Comparison of predicted and experimental pullout curves obtained at 500 °C after a 500 °C firing for a fibre inclination angle of 60°.

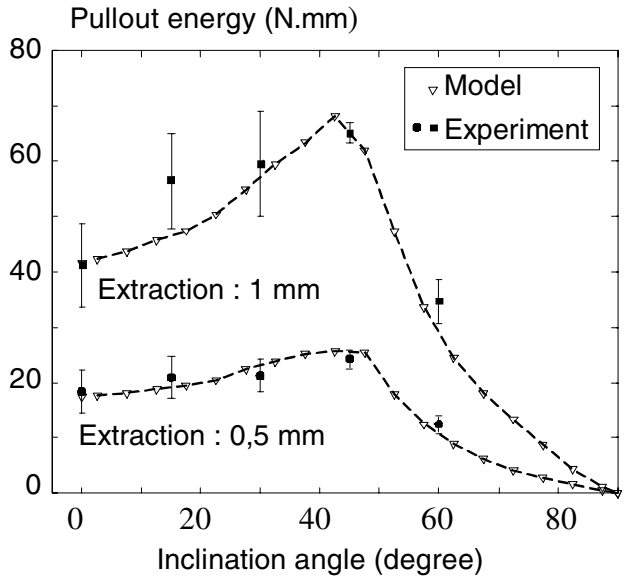

Fig. 15. Comparison of model predictions with experimental results in the case of pullout tests performed at room temperature after a 80 °C firing.

room temperature after a 80 °C firing and at a temperature test of 500 °C after a 500 °C firing. For these two conditions a good agreement is obtained between computed and experimental results, as well as the curves shapes and the pullout load amplitude. Matrix spalling can be identified by the large drops of the pullout load. It can be observed that the modelling can predict the matrix spalling with a good accuracy. The calculated displacements and the loads drops induced by matrix spalling correspond to those obtained experimentally for the two test conditions.

From the computed pullout curves, fibre extraction energies were calculated for numerous inclination angles between 0° and 90° and for fibre extraction values of 0.5 and 1 mm. Figs. 15–17 compare these predicted pullout energies with experimental results obtained for fibre inclination angles of 0°, 15°, 30°, 45° and 60°. Each experimental point is the average value of four pullout tests. For Figs. 15 and 16, the tests were performed at room temperature after a 80 °C firing and after a 500 °C firing. For Fig. 17, tests were performed at 500 °C after a 500 °C firing.

In Figs. 15 and 16 a good agreement between the calculated curves and the experimental points is shown all over the curves for the two considered

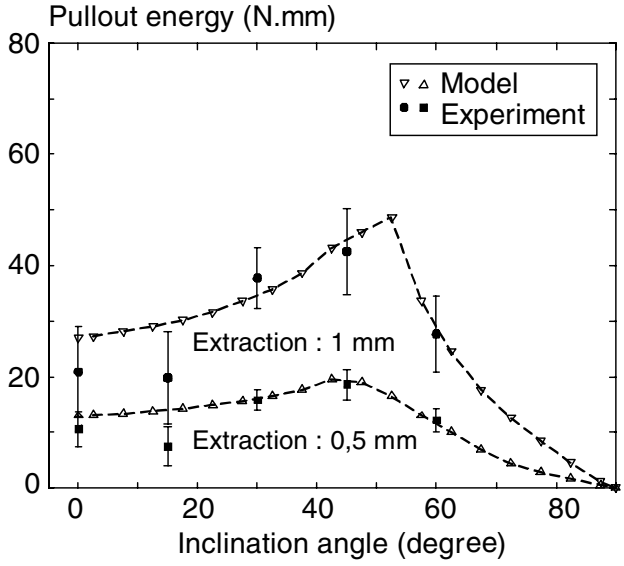

Fig. 16. Comparison of model predictions with experimental results in the case of pullout tests performed at room temperature after a 500 °C firing.

fibre displacements. In Fig. 17, a similar evolution of the experimental and the calculated pullout energy as a function of the inclination angle is noticed. Nevertheless, it can be observed that the calculated curve overestimates the fibre pullout

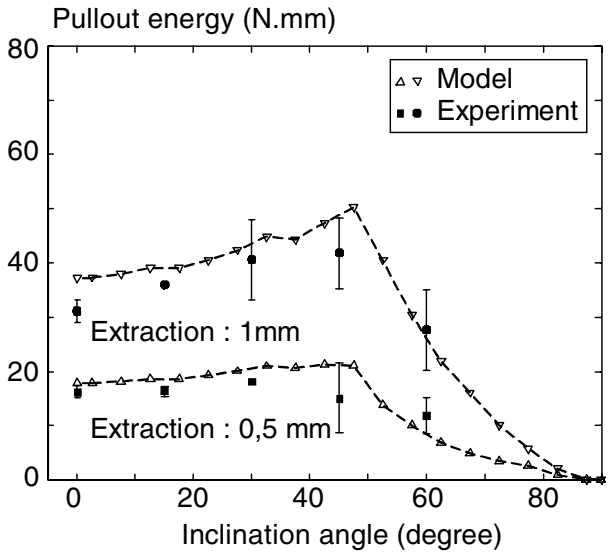

Fig. 17. Comparison of model predictions with experimental results in the case of pullout tests performed at 500 °C after a 500 °C firing.

energy for inclination values ranging from 0° to 50°. As described in Cailleux et al. (2002a,b), this overestimation can be explained both by the development of a fretting pressure at high temperature and by the emergence for low inclination angles of a stick-slip extraction mechanism which is not taken into account in this modelling.

The comparison of calculated and experimental curves demonstrates that the proposed model is able to predict both the pullout curves and the evolutions of the pullout energy as a function of the firing temperature, the testing temperature and the inclination angle. Such results allow to validate the modelling and the assumptions established to take into account the concentrated friction load at the fibre exit point and the mechanisms of matrix spalling, fibre bending and fibre extraction.

4.2. Parametric study for composite optimization

In this study, influences of both the friction coefficient and the unitary length of the spalled matrix element on the pullout curve were first considered. Then, evolutions of the pullout energy as a function of the fibre Young's modulus, the matrix rupture stress, the fibre embedded length, the firing temperature and the testing temperature were evaluated.

The effect of varying the friction coefficient value can be examined in Fig. 18. The increase of the friction coefficient leads to increase the pullout load and the matrix spalling load. These effects are more significant for high displacement values and are probably due to a fibre extraction locking. The evolution of the pullout load as a function of the friction coefficient is consistent with results obtained in previous works modelling the extraction of straight fibres (Kerans, 1991).

Fig. 19 shows the effect of varying the length (a_1) of the spalled matrix element on the pullout curve. The shape of the pullout curve is not affected and pullout load evolutions throughout the extraction process can be neglected. Nevertheless, it is seen from these plots that matrix spalling occurs for higher pullout displacement values and that the load drop amplitude increases when a_1 is raised from 0.37 to 0.75.

Fig. 20 shows the calculated pullout energy curves obtained with fibre Young's modulus of 100, 165 and 250 GPa. Varying this parameter provides pullout energy evolutions for inclination angles higher than 30°. An increase of the pullout energy can be observed when the fibre Young's modulus is increased. Otherwise, it can be noticed

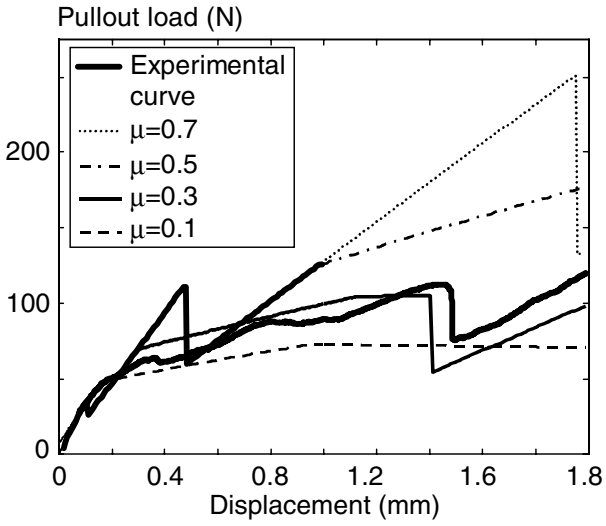

Fig. 18. Effect of varying the friction coefficient on the computed pullout curves and comparison with the experimental curve of a 80 °C fired sample.

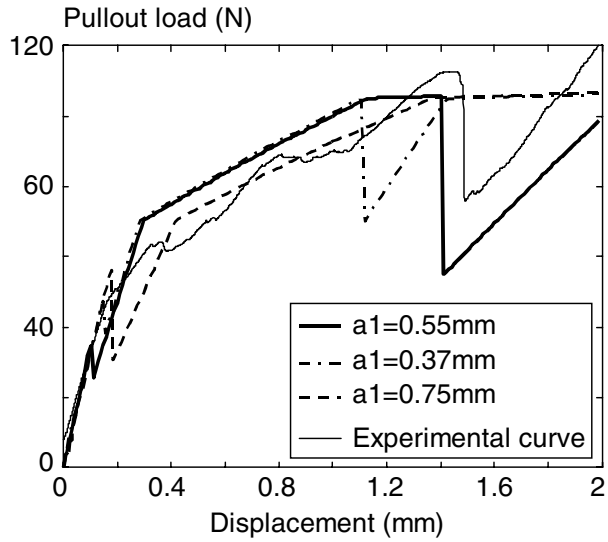

Fig. 19. Effect of varying the unitary length of the spalled matrix element on the computed pullout curves and comparison with the experimental curve of a 80 °C fired sample.

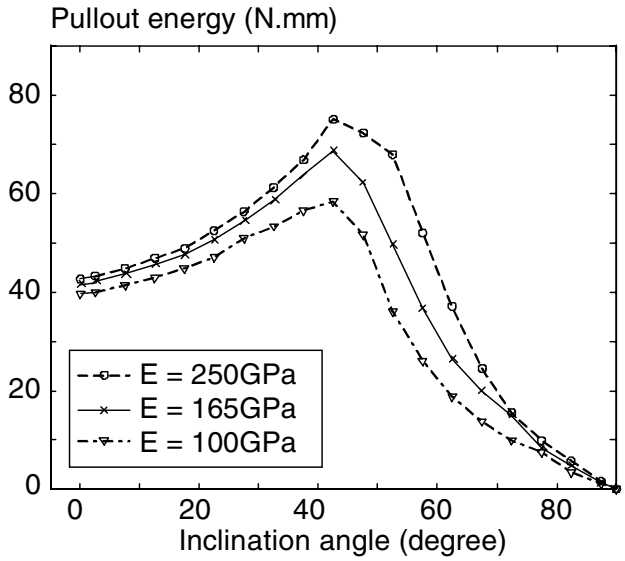

Fig. 20. Effect of fibre Young modulus on the calculated pullout energy curve as a function of the inclination angle.

that the inclination angle value corresponding to optimal pullout energy is not affected by this parameter. This value is close to 45° for all the considered conditions.

The fibre Young's modulus contribution is taken into account in this model to calculate the fibre bending and the fibre elastic deformation. As a consequence, it can be assumed that the displacement imposed at the beginning of a computing loop induces a higher fibre deformation in the inclination domain 30–90° than in the domain 0–30°. For low inclination angles, it may be supposed that the extraction is the more important contribution of the displacement of the fibre extremity. As a consequence, it may be concluded that high inclination angles provide a total or a partial fibre locking.

Fig. 21 illustrates the effect of the concrete rupture stress on the pullout energy curves. As for the fibre Young's modulus, this parameter induces important evolutions of the pullout energy for inclination angles higher than 30°. For lower values the effect of the concrete rupture stress can be neglected. Otherwise, an increase of the optimal inclination angle value can be observed when increasing the concrete rupture stress. This value is close to 37° for a rupture stress of 5 MPa and increases up to 50° for a rupture stress of 25 MPa. This phenomenon can be understood from the next two assumptions: concrete rupture stress variations provide evolutions of the number and dimensions of matrix spallings and, as it is observed in Fig. 18, load drops induced by matrix spalling provide significant lost of pullout energy.

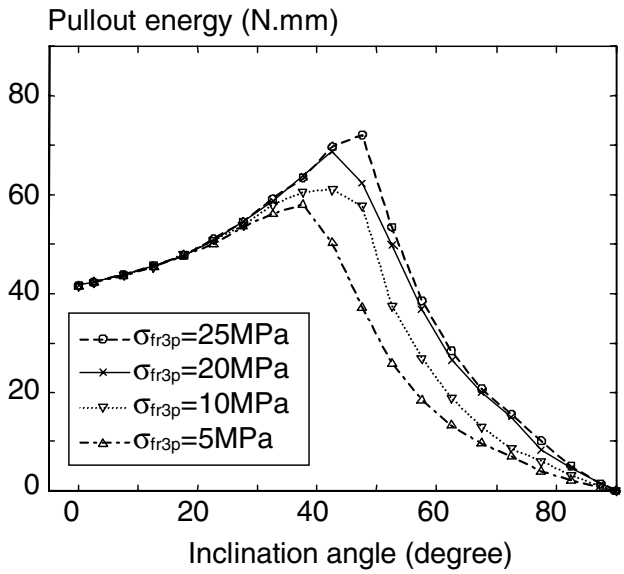

Fig. 21. Effect of concrete rupture stress on the calculated pullout energy as a function of the fibre inclination angle.

Therefore, the higher the concrete rupture stress is, the more difficult the matrix spalling for a given angle becomes and the higher the corresponding pullout energy is. In addition, for inclination angles in the 40–90° domain, an increase of the calculated pullout energies with the rupture stress reaches critical values. In this way, increase of the pullout energy obtained for a rupture stress fixed at 25 MPa is very limited in comparison with those corresponding to the 20 MPa one. This evolution suggests that the amplitude of matrix spalling mechanism induced with a rupture stress of 20 MPa is close to those obtained with 25 MPa. Therefore, for a given strength domain, matrix spalling becomes limited.

Fig. 22 shows the calculated pullout energy curves obtained by varying the fibre embedded length, the heat treatment temperature and the testing temperature. The pullout energy curve corresponding to a 500 °C heat treatment, a 500 °C tests and assuming a fibre embedded length of 12 mm was computed from the pullout model. For this modelling, the parameters F_{pic} and F_{flim} were determined from the values of τ_{pic} and τ_{flim} calculated for the case of a fibre embedded length of 6 mm. The parameters a, b, a_1 and μ were determined from the experimental results obtained from the same testing conditions with a fibre embedded length of 6 mm and were kept constant for a fibre embedded length of 12 mm.

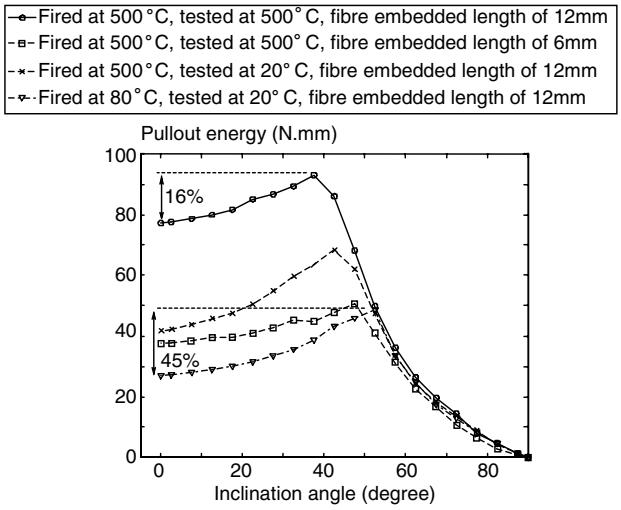

Fig. 22. Effect of fibre embedded length, heat treatment and temperature test on the calculated pullout energy as a function of the fibre inclination angle.

Considering the effect of the embedded fibre length, the superposition of the pullout energy curves calculated for a heat treatment of 500 °C, a testing temperature of 500 °C and embedded fibre lengths of 6 and 12 mm shows that for inclination angles lower than 40° the pullout energy can be increased by a factor of 2 between these two embedded lengths. For inclination angles ranging from 40° to 50°, this positive effect decreases progressively and beyond 50° the pullout energies determined for embedded lengths of 6 and 12 mm are very close. In the 50–90° inclination domain, the influence of the fibre embedded length on the pullout energy is negligible.

Considering the effect of the heat treatment (80 and 500 °C) and the testing temperature (20 and 500 °C), the computed curves show a significant evolution of the pullout energy as a function of these parameters essentially for inclination angle lower than 50°. In this way, for a straight embedded fibre the pullout energy is around 4 N mm after a 80 °C firing, decreases to 3 N mm after a 500 °C firing, and increases to 8 N mm for a test temperature of 500 °C. Moreover, it can be observed that the effect of the inclination angle on the fibre pullout energy depends on the firing and the testing temperatures. For example, the fibre inclination can increase the pullout energy at the most by 45% in the case of a room temperature test performed after a 500 °C firing and only by 16% in the case of tests performed at 500 °C. Otherwise, for fibre inclination higher than 50°, the amplitude and the shape of the pullout energy curves are similar. In the 50–90° inclination domain, pullout energy does not depend neither on the fibre/matrix interface nor on the heat treatment and nor on the testing temperature but only on the fibre inclination angle. This conclusion is confirmed by the extracted fibre lengths calculated by the model for all the considered test conditions. In this way, it appears that there is no fibre extraction for inclination angles between 50° and 90°. Consequently, the fibre extremity displacement is only caused by elastic strain and bending of the two beams system.

5. Conclusion

In this study, the fibre pullout behaviour from a reinforced refractory castable was characterized and modelled. In the first part, the effects of the firing temperature, the testing temperature and the inclination angle on the fibre pullout behaviour were investigated by high temperature pullout tests and scanning electron microscopy observations. It was established that the firing process leads to a decohesion of the fibre/matrix interface caused by the thermal expansion mismatch between the two components. As a consequence, a decrease of the fibre pullout load was observed when the firing temperature increases.

The high temperature tests showed an increase of the pullout mechanical performances. This phenomenon is induced by the development of a fretting pressure at the fibre/matrix interface.

The influence of the fibre inclination was quantified as a function of the testing and the firing temperature too. For all the considered conditions, similar evolutions were observed concerning the pullout load and the pullout energies: the pullout performances increase up to angles within 30–45° and decrease for higher inclination angles. The fibre pullout mechanisms induced by fibre inclination such as the fibre bending, the matrix spalling and the development of a local friction load at the fibre exit point were identified by SEM and optical microscopy observations.

In the second part, an analytical model of the fibre pullout was developed taking into account the previously described micromechanisms. This model is based on the strength of materials theory and is composed of two major domains. The first domain considers the fibre length outside the matrix and models the fibre bending. The second domain considers the fibre segment embedded inside the matrix and models the development of a friction load and the mechanisms of fibre extraction and matrix spalling. The model needs nine parameters and is based on a physical approach. Nevertheless, the experimental pullout tests of a straight fibre and of a 45° inclined fibre are necessary to determine the value of the friction coefficient and the elementary length of the spalled matrix element. Comparisons of calculated and experimental pullout curves and pullout energy curves showed that the model can predict the pullout behaviour as a function of the firing temperature and of the testing temperature with a good accuracy. A parametric study was then performed to evaluate and to discuss the effect of the material properties and of the temperature on the pullout performances. The effect of the following parameters was assessed: friction coefficient, length of the spalled matrix element, Young's modulus, rupture stress of concrete, and the testing and the firing temperatures.

References

Bartos, P., 1982. Bond in glass reinforced cements. In: Bond in Concrete, International Conference, Paisley, pp. 60–72.

Bartos, P.J.M., Duris, M., 1994. Effects of the inclinations of steel fibres to a tensile load on their loadbearing capacity and the SFRC fracture mechanism. In: Brandt, A., Li, V.C., Marshall, I.H. (Eds.), Brittle Matrix Composites 4. IKE and Woodhead, Warsaw, pp. 320–331.

Baumberger, T., Heslot, F., Perrin, B., 1994. Crossover from creep to inertial motion in friction dynamics. Lett. Nature 367, 544–546.

Baumberger, T., Caroli, C., Perrin, B., Ronsin, O., 1995. Nonlinear analysis of the stick-slip bifurcation in the creep-controlled regime of dry friction. Phys. Rev. E 51, 4005–4010.

Cai, H., Faber, K.T., 1992. Crack bridging by inclined fibers whiskers in ceramic composites. J. Am. Ceram. Soc. 75, 3111–3117.

Cailleux, E., 2001. Microstructure et comportement thermomécanique d'un béton réfractaire renforcé par des fibres métalliques. Ph.D. Thesis, Ecole des Mines de Paris, p. 241.

Cailleux, E., Cutard, T., Bernhart, G., 2002a. Study of a ceramic refractory reinforced with metallic fibres: from the microstructure to the mechanical behaviour. In: Proceedings of the CIMTEC 2002, Florence.

Cailleux, E., Cutard, T., Bernhart, G., 2002b. Pullout of metallic fibres in a ceramic refractory matrix. Compos. Part A Appl. Sci. Manuf. 33, 1461–1466.

Cutard, T., Cailleux, E., Lours, P., Bernhart, G., 1999. Structural and mechanical properties of a refractory concrete for superplastic forming tools. Ind. Ceram. 19, 100–102.

Davidovits, J., 1999. Chemistry of geopolymeric systems terminology. In: Proceedings of Geopolymer'99 Conference, Saint Quentin, pp. 9–39.

Helfet, J.L., Harris, B., 1972. Fracture toughness of composites reinforced with discontinuous fibres. J. Mater. Sci. 7, 494–498.

Katz, A., Li, V.C., 1995. Inclination angle effect of carbon fibers in cementitious composites. J. Eng. Mech. 121, 1340–1348.
Kerans, R.J., 1991. Theoretical analysis of fiber pullout and pushout tests. J. Am. Ceram. Soc. 74, 1585–1596.
Khanna, S.K., Shukla, A., 1994. Influence on fiber inclination and interfacial conditions on fracture in composite materials. Exp. Mech. 34, 171–180.
Leung, C.K.Y., Chi, J., 1995. Crack-bridging force in random ductile fiber brittle matrix composites. J. Eng. Mech. 121, 1315–1324.
Leung, C.K.Y., Li, V.C., 1992. Effect of fiber inclination on crack bridging stress in brittle fiber reinforced brittle matrix composites. J. Mech. Phys. Solids 40, 1333–1362.
Leung, C.K.Y., Ybanez, N., 1997. Pullout of inclined flexible fiber in cementitious composite. J. Eng. Mech. 123, 239–246.
Li, V.C., Wang, Y., Baker, S., 1990. Effect of inclining angle, bundling and surface treatment on synthetic fibre pull-out from a cement matrix. Composites 21, 132–140.
Morton, J., Groves, G.W., 1974. The cracking of composites consisting of discontinuous reinforced concrete. J. Mater. Sci. 9, 1436–1445.
Naaman, A.E., Shah, S.P., 1976. Pull-out mechanism in steel fiber-reinforced concrete. J. Struct. Div. 102, 1537–1548.
Ouyang, C., Pacios, A., Shah, S.P., 1994. Pullout of inclined fibers from cementitious matrix. J. Eng. Mech. 120, 2641–2659.
Shah, S.P., Ouyang, C., 1991. Mechanical behavior of fiber-reinforced cement-based composites. J. Am. Ceram. Soc. 74, 2727–2953.